COMSOL Multi-physics model for Transition Metal Dichalcogenides (TMD's)-Nafion composite Based Electromechanical Actuators

by

Ronit Prasad Sawant

A Thesis

Submitted to the Faculty

of the

WORCESTER POLYTECHNIC INSTITUTE

in partial fulfillment of the requirements for the

Degree of Master of Science

in

Mechanical Engineering

August 2018

APPROVED:

_____
Professor Balaji Panchapakesan, Advisor

_____
Professor Pradeep Radhakrishnan, Committee Member

_____
Professor Mehul A. Bhatia, Committee Member

_____
Professor Yuxiang Liu, Graduate Committee Representative

Abstract

The ability to convert electrical energy into mechanical motion is of significant interest in many energy conversion technologies. For more than a decade Ionic polymer-metal composite (IPMC) as an electroactive smart polymer material has been extensively studied and has shown great potential as soft robotic actuators, artificial muscles and dynamic sensors in the micro-to-macro size range. IPMC consists of an ion exchange polymer membrane sandwiched between two noble metal electrodes on either side of the membrane. Under applied potential, the IPMC actuator results in bending deformation because of ion migration and redistribution across its surface due to the imposed voltage. Nafion are highly porous polymer materials which have been extensively studied as the ion exchange membrane in IPMC. Nafion has also been mixed with carbon nanotubes, graphene, and metallic nanoparticles to improve actuation and bending characteristics of electro-mechanical actuators. For the first time, liquid phase exfoliated Transition Metal Dichalcogenides (TMDs)-Nafion nanocomposite based electro-mechanical actuators has been studied and demonstrate the improvement in the electromechanical actuation performance.

In this thesis, we create a 2D model of the TMD-Nafion based electromechanical actuator in COMSOL Multi-physics software. The behavior of the model is examined at different electric potentials, frequencies, and actuation lengths. The simulation results were compared with the experimental data for validation of the model. The data showed improvement in the actuation for TMD-Nafion actuator when compared with pure Nafion actuator. The improvement in the actuation was due to the increase in diffusivity of the TMD-Nafion actuator in comparison with pure Nafion actuator. This increase in the diffusivity as seen in the model is because of the new

proton conducting pathways being established with the addition of TMDs. The model also shows an increase in the stress and strain values with the incorporation of TMDs. With the same length of the actuator we were able to obtain more stress and strain with the addition of TMDs. This helps in improving the performance of the actuator as it would be able to handle more stress cycles which also increases the life of the actuator.

Acknowledgment

First of all, I would like to thank my thesis advisor Professor Balaji Panchapakesan for all of his support, patience and guidance during my Master's thesis at Worcester Polytechnic Institute.

I would like to thank Professor Pradeep Radhakrishnan, Professor Mehul Bhatia and Professor Yuxiang Liu for their valuable inputs and suggestion and for being there as a committee member.

I would also like to thank the office of Academic and Research Computing at WPI for providing me access to high performance computers.

Finally, I must express my gratitude to my parents and my family for providing me with unfailing support and continuous encouragement throughout my years of study. This accomplishment would never have been possible without them.

Table of Contents

List of figures

List of tables

List of Symbols

C   Cation Concentration

F   Faraday constant

z   Charge number

D   Diffusion constant

ϕ Electric Potential

P solvent Pressure

p   Polymer pressure

μ Mobility

R   Gas constant

T   Absolute temperature

ε effective dielectric permittivity

ρ Charge density

ρ_p Material density

C_a Anion concentration

C_o Initial anion or cation concentration

F Force per unit volume

E   Young's modulus

ν Poisson's ratio

u   local displacement vector

δ Polymer domain

ψ_1 & ψ_2 are the electrode domains

$\phi_{\partial\delta2}$ & $\phi_{\partial\delta4}$ are boundary condition at the electrode-polymer.

$\partial\delta_{1-4}$ are the polymer boundaries

$\partial\psi_1$ and $\partial\psi_2$ are boundaries of applied electric potential.

j   Electric current density vector in electrodes

V_{pos} and V_{neg} are applied electric potentials.

t   Thickness of the actuator

δ   Lateral displacement of the actuator

L   the free length of the actuator

ϵ_{max} Maximum strain

ϵ Strain

σ   Stress induced

Chapter 1

Introduction

The ability to convert electrical energy into mechanical motion is highly desirable for energy conversion, actuation, robotics and reconfigurable technologies. Today, a wide variety of smart technologies has been developed based on the conversion of electrical to mechanical energy which is used broadly from simple home blenders to complex aerospace technologies. Materials such as piezoelectrics [1], ferroelectrics [2], shape memory alloys [3] and electroactive polymers [4–7] are used as actuators that convert electrical energy into mechanical output.

Ionic polymer-metal composite (IPMC) is one such electroactive smart polymer material that has been extensively studied for more than a decade [8] and has shown great potential as soft robotic actuators, artificial muscles and dynamic sensors in the micro-to-macro size range [9]. IPMC consists of an ion exchange polymer membrane sandwiched between two noble metal electrodes on either side of the membrane. Under the application of an external voltage (0.5-5 V), the IPMC actuator results in bending deformation because of ion migration and redistribution across its surface due to the imposed voltage. The ion exchange membrane in IPMC are usually highly porous polymer materials, such as Nafion, but in some cases, other polymers such as Flemion have also been used [10]. Nafion is a sulfonated tetrafluoroethylene based fluoropolymer-copolymer with high porosity and unique ionic properties and was initially developed as electrolytic separators [22]. They have found applications in diverse areas such as ion exchange membranes [23], proton conductors [24], drug delivery [25], batteries [26] and in fuel cells [27] due to their

1

excellent mechanical properties, stability, electro-activity, water nanochannels and low cost. There are two types of IPMC: water-based and ionic liquid-based, the water-based IPMC require an aquatic environment to function where the current is caused by ions such as Na (+) and K (+) being dissociated in water whereas the ionic liquid-based IPMC does not require fluid medium to function [11]. The composite has excellent chemical and mechanical stability, high ionic conductivity, gas impermeability [12] and also biocompatible [13,14]. Now with the advent of nanomaterials such as carbon nanotubes [15] and graphene [16], they have also been explored in their native form as electrical actuators [17] and also by mixing them in different matrices to make nanocomposites [18–20]. Nafion has been mixed with carbon nanotubes [19], graphene [20], and metallic nanoparticles [21] to improve actuation and bending characteristics of electro-mechanical actuators. Recently, semiconductors such as Transition Metal Dichalcogenides (TMDs) have found various applications as transistors [28], optoelectronic devices [29], photo-thermal actuators [30] and solar cells [31]. Transition Metal Dichalcogenides are the class of 2D layered materials with transition metal layer between two chalcogen layers. The atoms within the layers are bonded through strong covalent bonds [32]. Layered materials represent a diverse and largely untapped source of two-dimensional (2D) systems with exotic electronic properties and high specific surface areas that are important for sensing [33], catalysis [34], energy storage [35], and actuation applications [36]. However, they have not been evaluated as electro-active materials in Nafion polymer actuators. But for the first time Loeian et al. [37] incorporated TMDs such as WS_2 in Nafion and demonstrate the improvement in the electromechanical actuation performance.

The goal of this thesis is as follows:(1) Model the TMD-Nafion based electromechanical actuator in COMSOL Multi-physics software ;(2) Simulate the results and compare it with the experimental

data for validation of the model;(3) Examine the behavior of the actuator model at different frequencies and electric potentials and analyze their effect on the actuation ;(4) Investigate the performance of the actuator at different actuation length.

This thesis is organized into the following chapters:

In Chapter 2, we present the background and summarizes the current state of the art research on IPMC actuators. It summarizes various techniques used to build the actuator and also use of various materials with Nafion to improve the actuation performance.

In Chapter 3, we present the mathematical model for the actuator. This includes the governing equation used. The Boundary conditions that are used to solve the governing equation. Also discussion regarding mesh and solver selection.

In Chapter 4, we study the computational results for a Nafion Based electromechanical actuator. The approach used to implement the model in COMSOL is discussed. The model is analyzed for different electric potentials, frequencies and actuation length.

In Chapter 5, we study the computational results for a TMDs-Nafion Based electromechanical actuator. The approach used to implement the model in COMSOL is discussed. The model is analyzed for different electric potentials, frequencies and actuation length. Through results it is shown how the incorporation of TMDs in Nafion improves the actuation performance.

Chapter 6 concludes the thesis and provides directions for future studies on electromechanical actuator based on Nafion and TMDs.

Chapter 2

Background

The basic model of the actuator can be seen in Figure 1. It consists of polymer membrane which is formed by fixed anions (Polymer Backbone) and free cation along with some water molecules sandwiched between two metal electrodes. The first conceptual fundamental design was reported in 1991 by Shahinpoor et al. [38,39] in which the use of IPMC actuator in swimming robotic structure was proposed. A number of numerical models on IPMC actuator were presented by Segalman et al. [38,40] in which the diffusion equation describing the evolution of the solvent concentration and resulting strain of polymeric gel material was also proposed. This was followed by papers on finite element analysis of the polymeric gel materials [41,42]. Later, Shahinpoor et al. [43-45] demonstrated a non-homogeneous theory on large deformation of ionic polymer gels in electric filed. The presented model takes into account the spatial redistribution of the ions inside the material due to the applied electric potential. Also, the deformation was defined as a function of electric field strength, dimensions, and the material's physical parameters. De Gennes et al. [46] describe the ion mechanism based on linear irreversible thermodynamics for sensing and actuation. Using a micromechanical model, the effect of cluster morphology of Nafion on electro-elastic moduli and ion conductivity was studied by Nemat-Nasser and Li [47]. The correlation between the actuation property with the capacitance of the transducer was studied by Akle et al. [48]. They showed that strain response and capacitance are strongly correlated and have a linear relation between them. Toi and Kang made used of Galerkin method for their FEM model and also incorporated viscosity term during transportation process into the FEM model [49].

Wallmersperger et al. [50] reported that by increasing the dielectric permittivity value and diffusion constant, large surface area effect of the electrode could be used in the ion transport model.
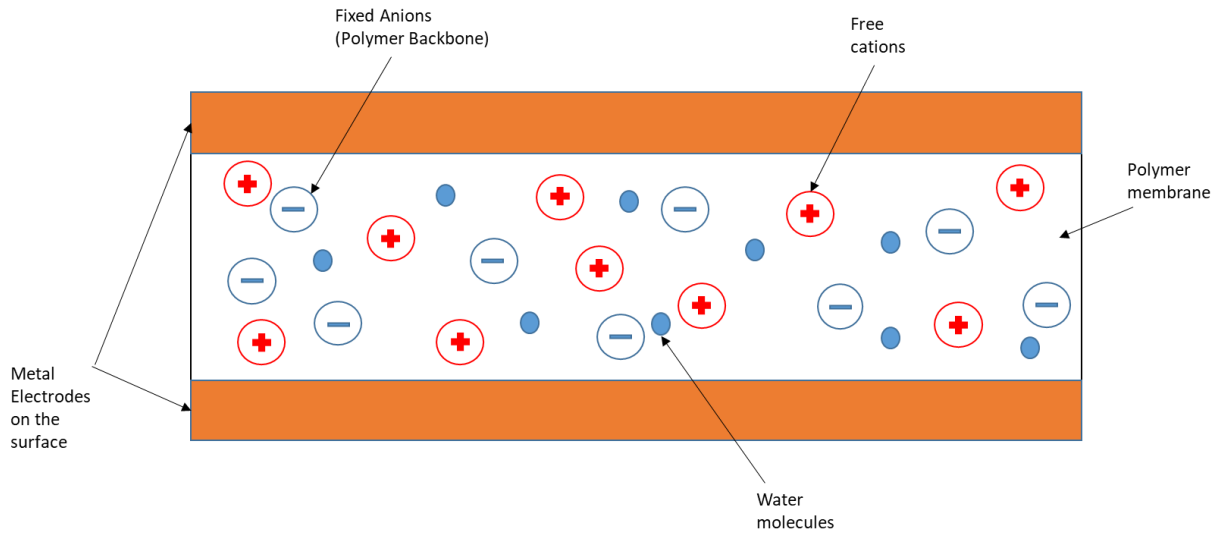
Figure 1: Conceptual diagram of the actuator

Akle et al. showed that higher electrode surface area results in more stored charge by analyzing numerically and experimentally the high surface area effect on the induced current [51]. Pugal et al. incorporated the effect of the electrode in the model of the actuator using the Ramo-Shockley theorem [52]. The model couples the current in the polymer with the electric current in the electrodes of the actuator which helps in improving the overall accuracy of the model. Martinez and Lumia presented a model for arbitrarily shaped ionic polymer–metal composite actuators [53] which predicts force output of three-dimensional actuators of arbitrary dimension. Vokoun et al. [54] demonstrated blocking force for different thicknesses in this 3D finite element model. It showed that the maximum blocking force increases with the increase in thickness of the polymer membrane. Landi et al. [19] showed improvement in conductivity and displacement by

5

incorporating nanotubes in Nafion. Jung et al. [20] studied the interaction mechanism between graphene and Nafion, showing improvement in the actuation performances. It was seen that the tensile strength of the graphene–Nafion ionic membrane was improved up to 200% within 1.0 wt.% loading, and Young's modulus was more than two times with a minute loading of graphene to Nafion electrolyte. Bian et al. [21] also showed improvement in the actuation behavior by incorporating metal nanoparticle in nafion. By doping $BaTiO_3$ nanoparticles in nafion, great improvement in deflection up to 101.4% under the dc input and 250% under the ac input at a frequency of 1 Hz were obtained. It is seen that due to their large strength, ability to modulate the conduction of electrons through doping and enhanced water uptake, TMDs can be used in the application for Nafion based electro-mechanical actuation technologies. Loeian et al. [37] incorporated TMDs such as WS_2 in Nafion and showed improvements in Young's modulus of 114% with the addition of 0.5 wt.% of TMDs in dry condition and 160% increase in proton conductivity with the addition of 0.5 wt.% TMDs in Nafion.

Chapter 3

Modeling of the Electromechanical Actuator in COMSOL Multi-Physics

3.1 Introduction

In this chapter, we present the mathematical equation used to model the 2D electromechanical actuator in COMSOL. It begins with the governing equation used to define the underlying mechanism inside the material. The boundary condition used to solve the equation is studied. The mesh and solver selection are also discussed.

There are three basic phenomena which should be considered for the physical models of the IPMC actuators: (1) electric field change inside the actuator due to the distribution of mobile ions and the applied electric potential at the electrodes. (electrostatic problem); (2) Mass transfer (diffusive, migration and convective transports); (3) Occurrence of stress and strain due to redistribution of the ions and water in the IPMC [54]. The figure 2 shows the fundamental model of the IPMC as an actuator. It consists of the polymer membrane in between two metal electrodes. When applied by the electric potential the mobile cations are attracted towards the cathode causing the surface to expand which results in bending of the actuator towards the anode.
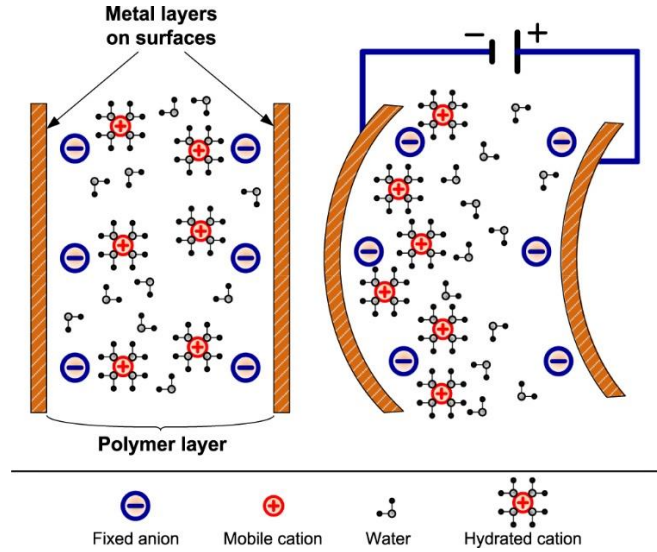
Figure 2: The fundamentals of an IPMC as an actuator [55]

3.2 Governing Equations:

The underlying cause of actuation is ion migration due to the applied electric field and resulting charge density in the vicinity of the electrodes.

The ionic current in the actuator is calculated with the Nernst–Planck equation:

$$\frac{\partial C}{\partial t} + \nabla \cdot (-D\nabla C - z\mu FC\nabla\phi - \mu C\Delta V\nabla P) = 0 \qquad (3.1)$$

Where C is the cation concentration, m is the mobility of cations, D is the diffusion constant, F is the Faraday constant, z is the charge number, ΔV is the molar volume that quantifies the cation hydrophilicity, P is the solvent pressure, and ϕ is the electric potential in the polymer. The Nernst–Planck equation is the main governing equation for describing the transduction phenomena of the IPMC materials.

For electromechanical actuation, the electric potential gradient term is significantly more prevalent than the solvent pressure flux, that is $zF\nabla\phi \gg \Delta V \nabla P$, therefore, the pressure flux term can be neglected in actuation model implementation [56]. But in sensing application, the term is of importance and should be considered while modeling.

This reduces the Nernst–Planck equation to

$$\frac{\partial C}{\partial t} + \nabla.\left(-D\nabla C - z\mu FC\nabla\phi\right) = 0 \tag{3.2}$$

The mobility in the equation is given by:

$$\mu = \frac{D}{RT} \tag{3.3}$$

where R is the gas constant and T is the absolute temperature.

The potential term ϕ is described by Poisson's equation as

$$-\nabla^2\phi = \frac{\rho}{\varepsilon} \tag{3.4}$$

where ρ is the charge density, which is defined as

$$\rho = F(C - C_a) \tag{3.5}$$

Here C_a is the anion concentration. The variable ε is the effective dielectric permittivity that can be explicitly written as $\varepsilon = \varepsilon_0\varepsilon_r$, where ε_0 is the dielectric permittivity in a vacuum and equals $8.85 \times 10^{-12}Fm^{-1}$.

It is seen that the cation concentration C is governed by Nernst–Planck equation while the anion concentration is related to the local volumetric strain as:

$$dV = \nabla.u \tag{3.6}$$

Here, u is the local displacement vector. A positive value of the volumetric strain indicates an increase in the local volume and negative indicates a decrease in the volume. As the anions are the part of the polymer backbone, changes in the volume in the polymer structure affect the local anion concentration. Therefore, the anion concentration is expressed in terms of volume as:

$$C_a = C_o(1 - dV) \tag{3.7}$$

where C_o is the initial cation or anion concentration. It must be noted that for most practical calculations it is reasonable to approximate $C_a = C_o$ [56].

The solvent pressure is caused by local strain in the polymer matrix, forcing the solvent from the concave side to the convex side of IPMC. Effective cation transport due to this term is governed by the pressure gradient ΔP and molar volume constant ΔV in the ionic flux term in Nernst–Planck eqn. Pressure P is the solvent pressure caused by the strain in the polymer. According to the momentum conservation, the solvent pressure and the pressure of the polymer p are related as follows [57]:

$$\nabla(P + p) = 0 \Rightarrow \nabla P = -\nabla p \tag{3.8}$$

It has been shown that [56]:

$$p(dV) = \frac{E(1 - v)}{(1 + v)(1 - 2v)} dV \tag{3.9}$$

where E is Young's modulus of the material and v is the Poisson's ratio.

By knowing those constants, Navier's equation can be constructed for displacements:

$$-\nabla.\sigma = F \tag{3.10}$$

With F being the force per unit volume. Newton's Second Law is used to describe time-dependent deformation:

$$\rho_p \frac{\partial^2 u}{\partial t^2} - \nabla.c\nabla u = F \tag{3.11}$$

where ρ_p is the density of the material and the second term is the static Navier's equation. The first term in eqn introduces the dynamic part.

In cases of electromechanical transduction, the body force F is defined as a function of charge density ρ:

$$F = f(\rho) \tag{3.12}$$

3.3 Boundary Conditions:

Here we present the boundary conditions which are used to solve the governing equations. Figure 3 represents the polymer domain, electrode domains and boundaries of the actuator model. The Nernst-Planck and Poisson equation is solved in Polymer domain δ and the domain ψ_1 & ψ_2 are used for the electrodes which are used to apply electric potential.
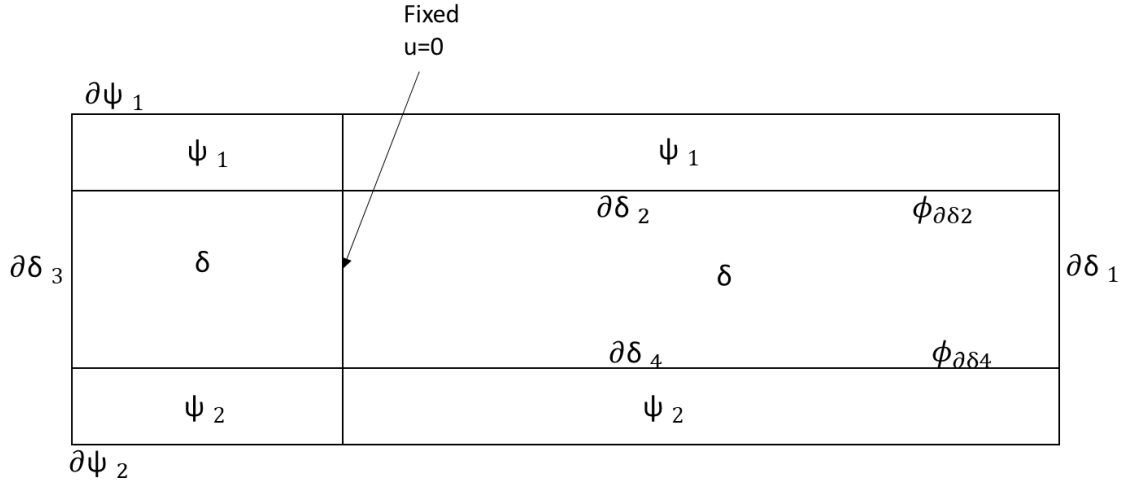
Figure 3: 2D electromechanical actuator model with all the boundaries and domains: δ is the polymer domain, ψ_1 & ψ_2 are the electrode domain, $\partial\delta_{1-4}$ are the polymer boundaries, $\phi_{\partial\delta2}$ & $\phi_{\partial\delta4}$ are boundary condition at the electrode-polymer interface, $\partial\psi_1$ and $\partial\psi_2$ are boundaries of applied electric potential.

The Boundary Condition used to solve the governing equation for the actuator are as follows:

For Nernst Plank Equation (3.2) for Domain δ at boundaries $\partial\delta_{1-4}$:

$$-D\frac{\partial C}{\partial n} - z\mu FC\frac{\partial \phi}{\partial n} = 0 \tag{3.13}$$

For the Poisson Equation (3.4) which is used to solve the potential inside the polymer:

- At boundary $\partial\delta_2$ and $\partial\delta_4$:

$$\phi_{\partial\delta4} = V, \phi_{\partial\delta2} = V \tag{3.14}$$

- At boundary $\partial\delta_1$ and $\partial\delta_3$:

$$\frac{\partial\phi_{\partial\delta3}}{\partial n} = \frac{\partial\phi_{\partial\delta1}}{\partial n} = 0 \tag{3.15}$$

For the Ohm's law in an electrode domain ψ_1 and ψ_2:

- sides that are in contact with polymer:

$$n.j = 0 \qquad\qquad (3.16)$$

- For contacts $\partial\psi_1$ and $\partial\psi_2$:

$$V_{\partial\psi_1} = V_{pos}, V_{\partial\psi_2} = V_{neg} \qquad (3.17)$$

where V_{pos} and V_{neg} are applied electric potentials. Here we applied the input square signal at V_{pos}, while V_{neg} is grounded.

3.4 Mesh and Solver Selection:

The selection of mesh plays a very important role in the determining the accuracy of the simulated results. Free triangular mesh or mapped mesh can be used for our model. The mapped mesh was used for our model. The advantage of using mapped mesh is that it provides more control over the element size and distribution compared to the free triangular mesh [56]. Also, the mapped mesh results in the generation of fewer elements which in turn reduces the simulation time. The model consists of a cantilever beam as shown in figure 4 which also shows the mesh distribution. The experiments were carried out on cantilever structured actuator because of which we made use of cantilever beam for our model in order to validate the model.

Time-dependent solver was used for our study. Since our input signal is a square wave which is periodic and the results changes with respect to time, time-dependent solver was the best option to

get optimum results. We performed the study into two parts: (1) Study 1 is used to simulate Transport of diluted species, Electric current, and General form PDE model which are used to solve for the ionic current and charge density throughout the polymer. (2) Study 2 is used to simulate the Structural Mechanics Module which is used to solve polymer deformation. For study 1, the number of elements in the mesh distribution was kept at 20 for the polymer membrane and for the electrode membrane the distribution is 2 and for study 2, the number of element in the distribution were kept at 1 for the polymer membrane and for electrode the distribution is 2. Here the number of element were selected based on the computational time and the accuracy of the results. It was seen that for the lower value of the elements the computational time considerably reduces but the accuracy of the model gets affected and at higher values the accuracy increases but the computational time is too long. Initially we started with 20 number of elements and got the desired mechanical responses such as displacement, stress and strain in accordance with the experiments and then we increased the value to 40. Here it was observed that error in the mechanical response are very small (less than 5%) when the elements are increased to 40. This also shows that the results are physical for number of elements between the range of 20-40. However, the computational time increases considerably with the increase in the number of elements. Therefore, in order to have accurate results and optimum computational time we selected the number of elements to be 20.
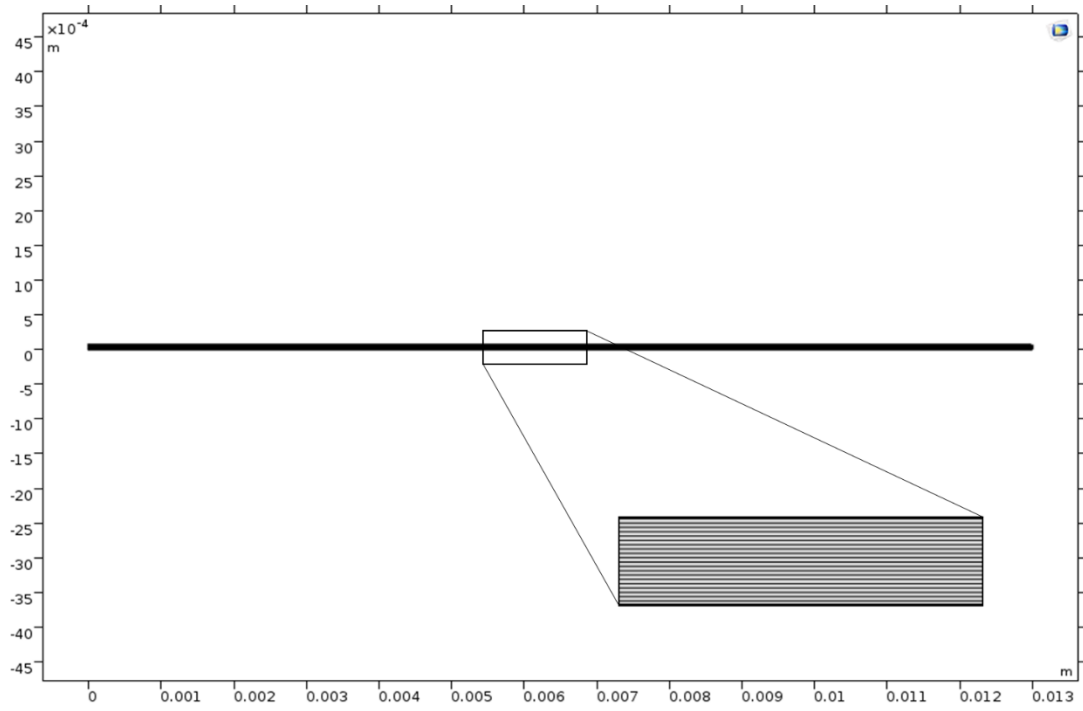
Figure 4: 2D cantilever actuator model. Mapped mesh technique has been used for the actuator.

Chapter 4

Computational Results for Pure Nafion Actuator

4.1 Introduction

In this chapter, we present the simulated results for the pure Nafion based actuator. These results work as a reference to compare it with the TMD-Nafion actuator which will be discussed later in Chapter 5. Now in order to incorporate the model in COMSOL we made use of 4 physics modules: (1) Transport of diluted species for Cation/anion concentrations, electric potential, and charge density (Nernst-Planck equation) (2) Electric current for electric voltage potentials in the metal electrodes (3) General form PDE to utilized for Poisson's equation for electric potential gradient and charge density. (4) Solid mechanics for the linear elastic material model. The geometry of the actuator model can be seen in Figure 5. It consists of a simple cantilever structure in which the polymer membrane is sandwiched between two electrodes. Table 1 shows the dimensions of the model. These dimensions of the model are taken from Loeian et al. [37] for the purpose of validating the simulated results with the experiments.
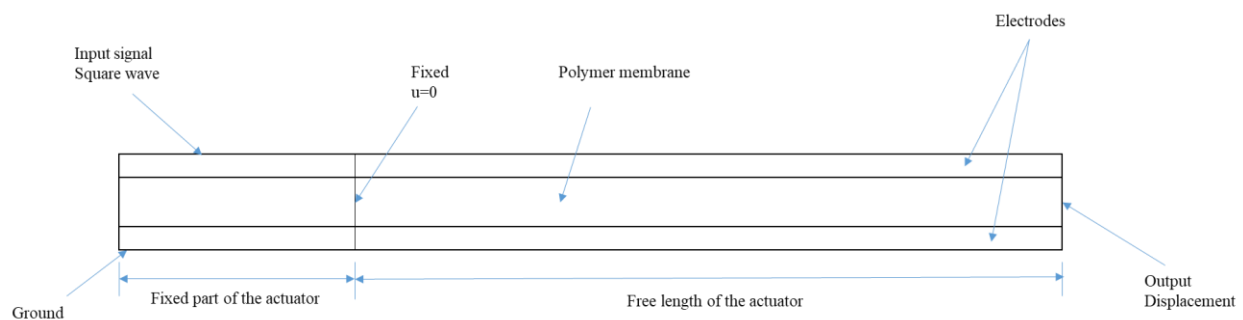

Figure 5: 2D cantilever model of the actuator in COMSOL

16

Free length of the actuator	10 mm
Length of the fixed part of the IPMC cantilever	3 mm
Thickness of the Actuator (Polymer Membrane)	0.07 mm
Thickness of the electrodes	0.0001 mm
Depth of the actuator (Width)	5 mm

Table 1: Geometric parameter of the Pure Nafion actuator

First, a 2V square wave electric potential at 1Hz is applied to the actuator. Now in order to get the displacement as close as possible to the experimental data from Loeian et al. [37], we adjust the cation concentration and diffusivity of the Nafion. Among the parameters used to define the actuator, we identify diffusivity and cation concentration to have a significant effect on the displacement of the actuator. All the other parameters are constants. Once we have the desired parameters for our model which produce the needed displacement. We simulate the results at different electric potential, frequencies and for various actuation lengths which are explained in detail in the following sections of this chapter. The parameters that are used to define the Nafion actuator are shown in Table 2.

Definition	Symbol (Used in Equations)	Symbol (As used in COMSOL)	Value	Units
Diffusivity or Diffusion constant	D	D_cat	5E-13	[m^2/s]
Charge Number	z	z_cat	1	
Gas constant	R	R	8.31	[J/(mol*K)]
Temperature	T	T	293	[K]
Cation concentration	C	conc_cat_conc	100	[mol/m^3]
Effective di-electric permittivity	ε	epsilon	2	[mF/m]
Density of the material	ρ_p	density_IPMC	2000	[kg/m^3]
Faraday constant	F	Faraday	96485.3415	[s*A/mol]
Young's Modulus	E	Young_IPMC	228.6	[Mpa]
Poisson's ratio	ν	Poission_IPMC	0.49	
Constant	α	Alpha	0.0001	[N/C]

Table 2: Parameters used in the modeling of the Pure Nafion actuator

4.2 Simulation Results:

Figure 6 shows the tip displacement of the actuator versus time under 2V square wave at 1Hz. The Length of the actuator was kept at 10mm. The high initial actuation is due to the electrochemical feedback which makes an initial fast electrically driven actuation followed by a slow actuation when the diffusive component of the chemical flux compensates for the effects of the electrical migrative component [58]. The displacement of the model is in good agreement with the experimental results. The model produces a displacement of ~ 0.128 mm at 2V for 10 mm actuation length in comparison to experimental displacement which is ~ 0.12 mm. Figure 7 shows the

18

concentration of cation across the thickness of the actuator at 2V 1Hz square wave. The result shows a large increase in ion concentration in a small subsurface region (<1µm) which therefore causes swelling of the polymer near cathode and contraction near the anode. This, in turn, results in bending of the material towards the anode. The accumulation of ions at the surface of the composite causes the elongation of the surface and deformation of the actuator. The bending in the actuator on the application of potential can be seen in figure 8. It also shows von Mises stress induced in the actuator due to the bending at 2V electric potential. The stress value here helps in analyzing the number of stress cycles the actuator can tolerate.
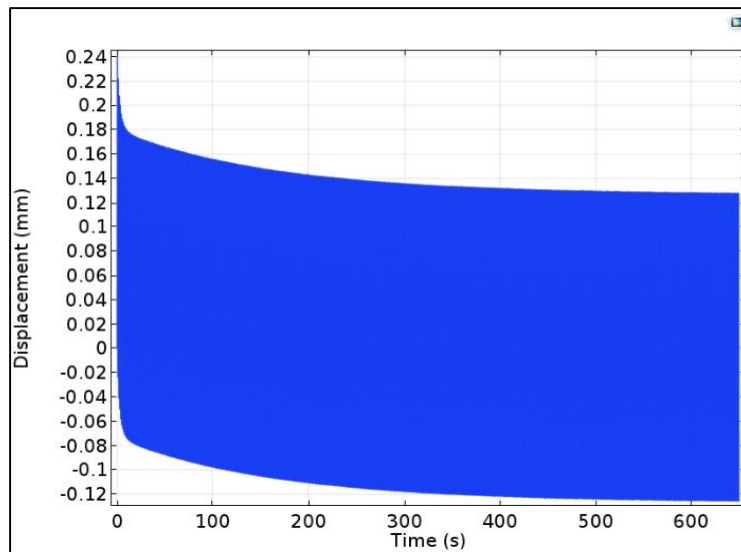
(a)
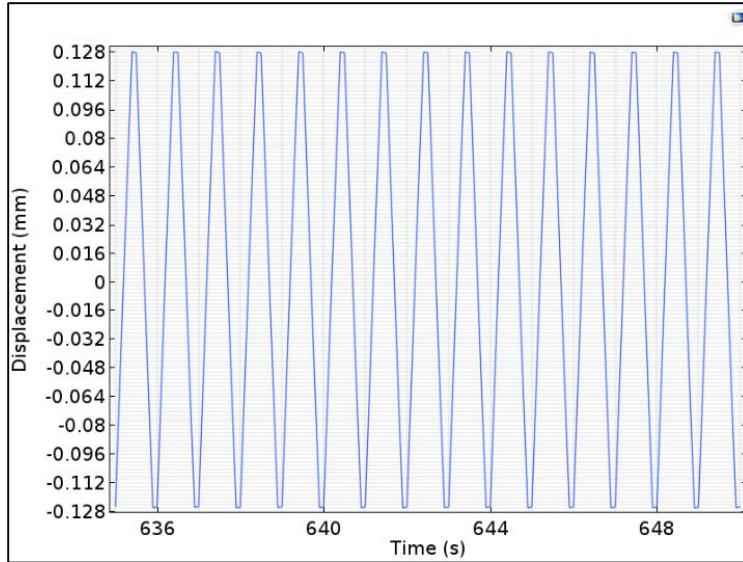
(b)

Figure 6: Tip displacement of the Nafion actuator under applied potential.(a) Displacement vs Time under 2V 1Hz square signal (b) Zoomed image of the tip displacement
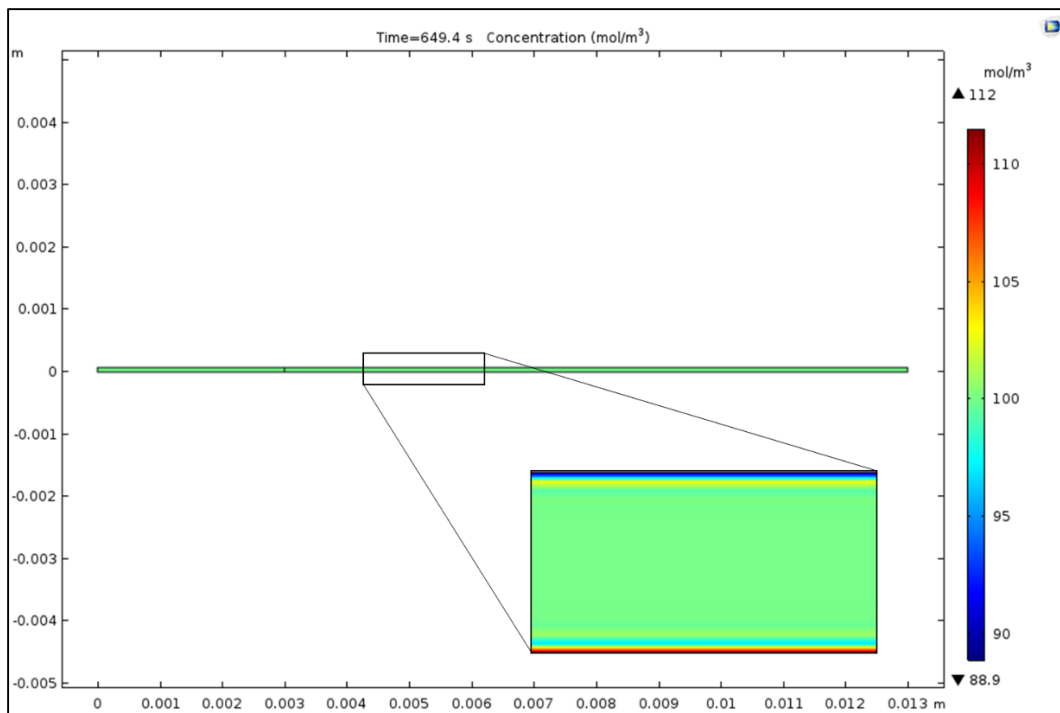
Figure 7: Cation concentration across the thickness of the Nafion actuator.
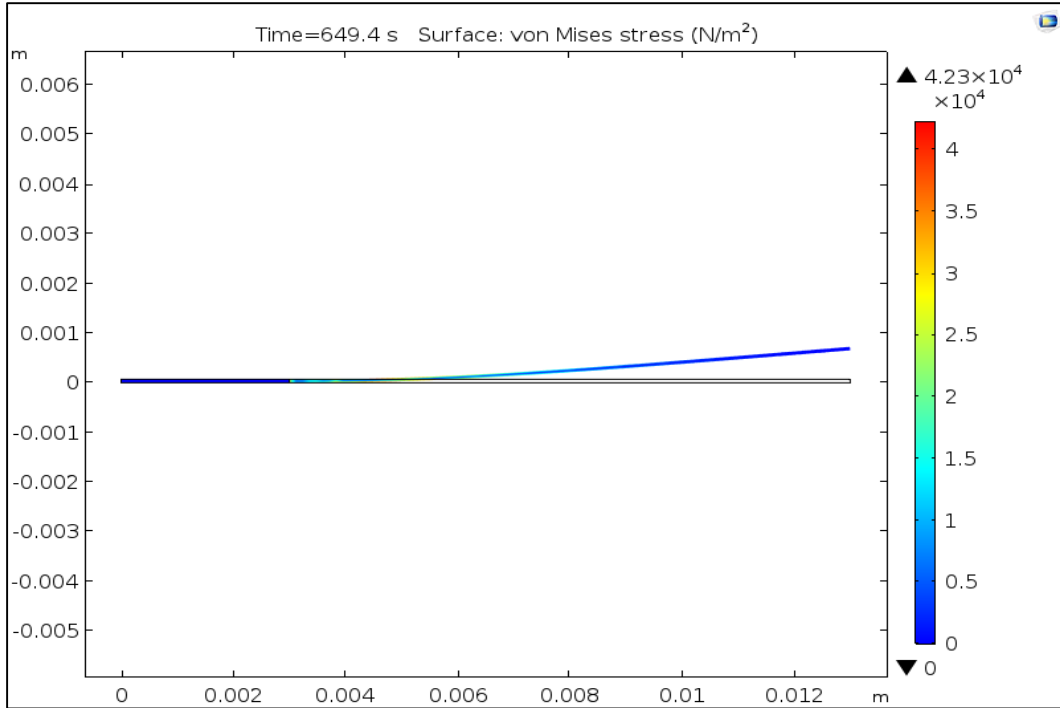
Figure 8: Von Mises Stress and bending of the Nafion actuator

4.3 Analyzing the Actuator at Different Electric Potential

Here the actuator performance is analyzed at different electric potential as seen in Figure 9. The parameters of the actuator shown in Table 2 are kept constant. The excitation frequency is kept at 1Hz, and the voltages are varied from 1V to 5V. The free length of the actuator was 10mm. Figure 9(a) shows displacement versus the electric potential for Nafion actuator. It can be seen that as the displacement increases with the increase in the electric potential. The stress and strain data with respect to the electric potential can be seen in Figure 9 (b) and (c). As the potential increases, the

stress as well as the strain increases. For large deformations, considering constant curvature, the maximum strain at the surface of the actuator is given by the following equation [37]:

$$\epsilon_{max} = \frac{2t\delta}{L^2 + \delta^2}$$

(4.1)

where t is the thickness, δ the lateral displacement of the actuator, and L is the free length of the actuator. The stress-strain relationship is

$$\sigma = E\epsilon$$

(4.2)

Where σ is the stress and ϵ is the strain.

(a)

(b)   (c)
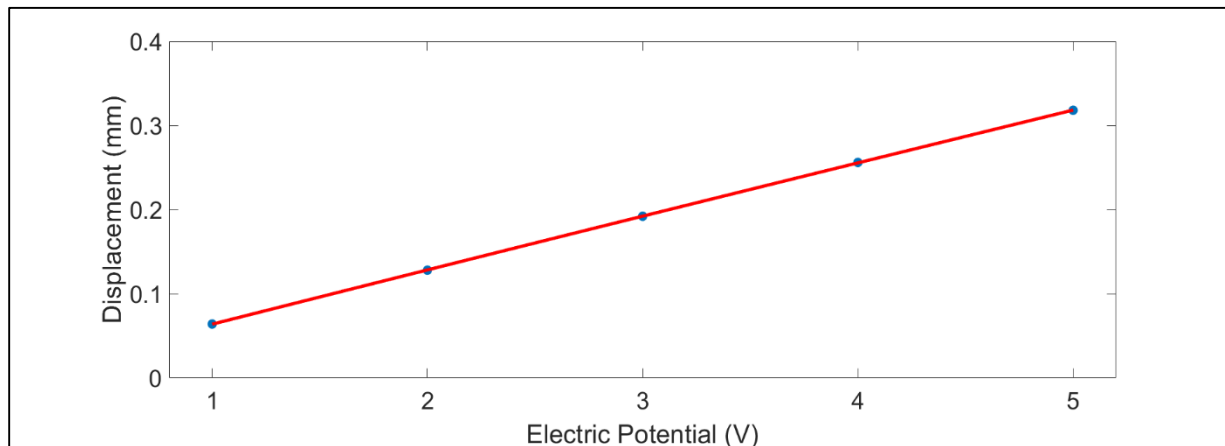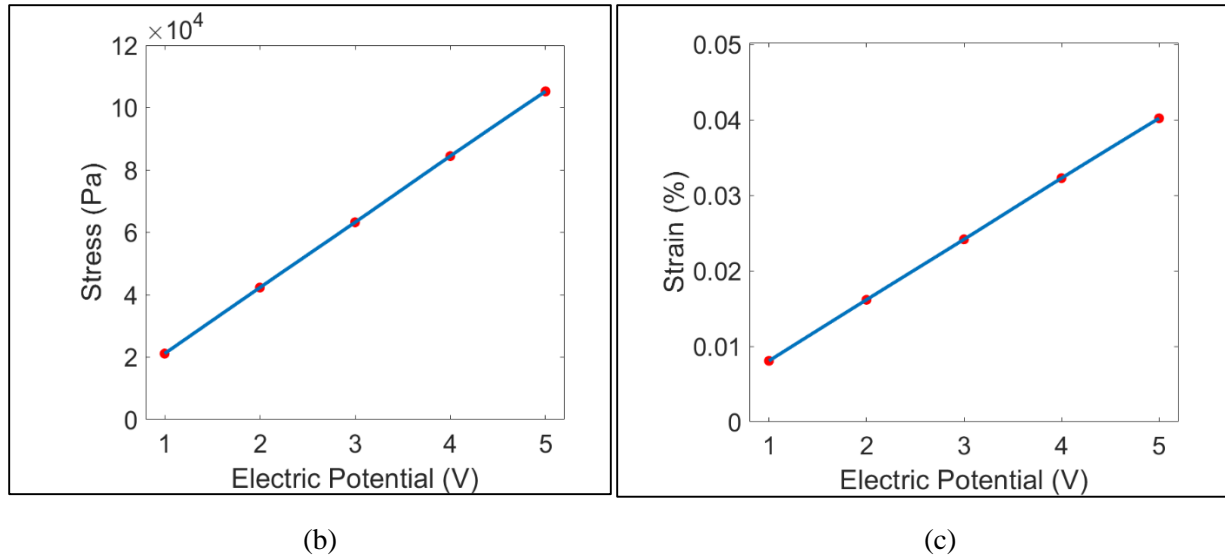
Figure 9: Mechanical response at different electric potential for Nafion actuator:(a)Displacement versus Electric potential (b) Stress versus Electric potential (c) Strain % versus Electric Potential

4.4 Analyzing the Actuator at Different Excitation Frequencies

Here we analyze the actuator at various excitation frequencies as seen in figure 10. The applied electric potential amplitude was kept at 2V for all frequencies. The actuation length is kept at 10 mm. Performance is studied at 0.1 Hz,1Hz, and 5Hz. Figure 9(a) shows how the displacement varies with the excitation frequencies. It is seen that as the excitation frequency increases the displacement of the actuator decreases. The stress and strain relationships with the excitation frequency can be seen in Figure 10(b) and (c) respectively.
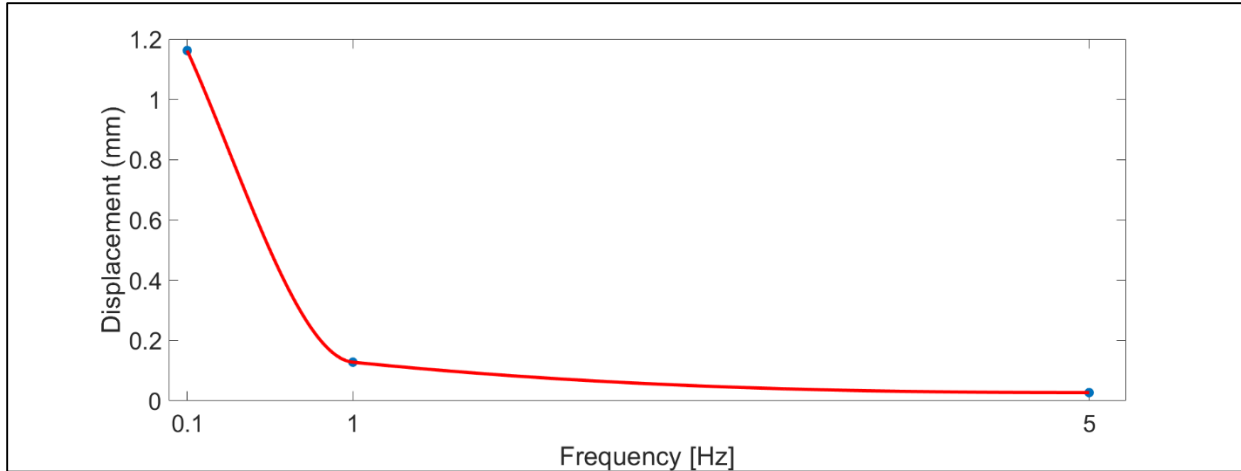
(a)
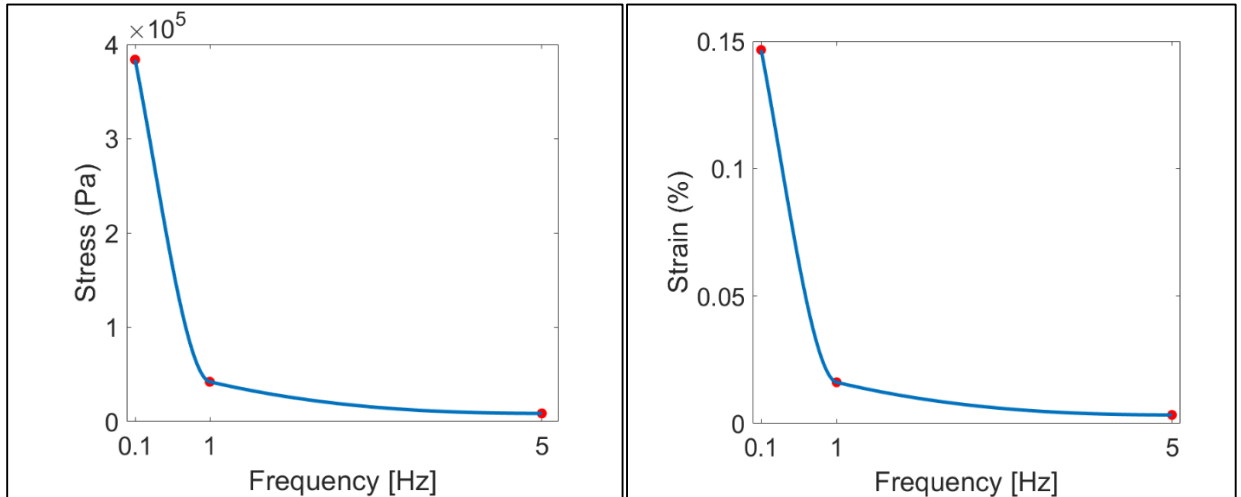
(b)   (c)

Figure 10: Mechanical response at different excitation frequencies for Nafion actuator:(a)Displacement versus frequency(b) Stress versus frequency (c) Strain % versus frequency

4.5 Effect of Varying Actuation Lengths

Here we analyze the actuator at different actuation lengths. The electric potential amplitude was kept at 2V 1 Hz for all actuators. Actuation length of 5mm, 8mm and 10mm were used to study the performance. Figure 11(a) shows the displacement versus actuation length plot. The displacement decreases with the decrease in the actuation length. The parameters were kept

constant for all the samples. The stress and strain relation for various length of the actuator can be seen in Figure 11(b) and (c) respectively. Also, as the actuation length increases the stress and strain increases.
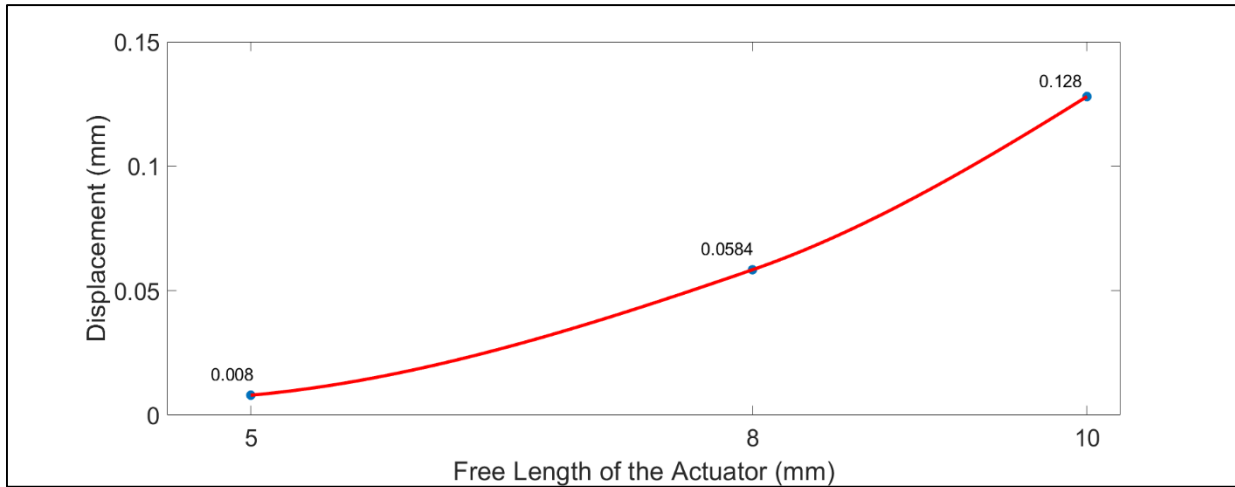
(a)
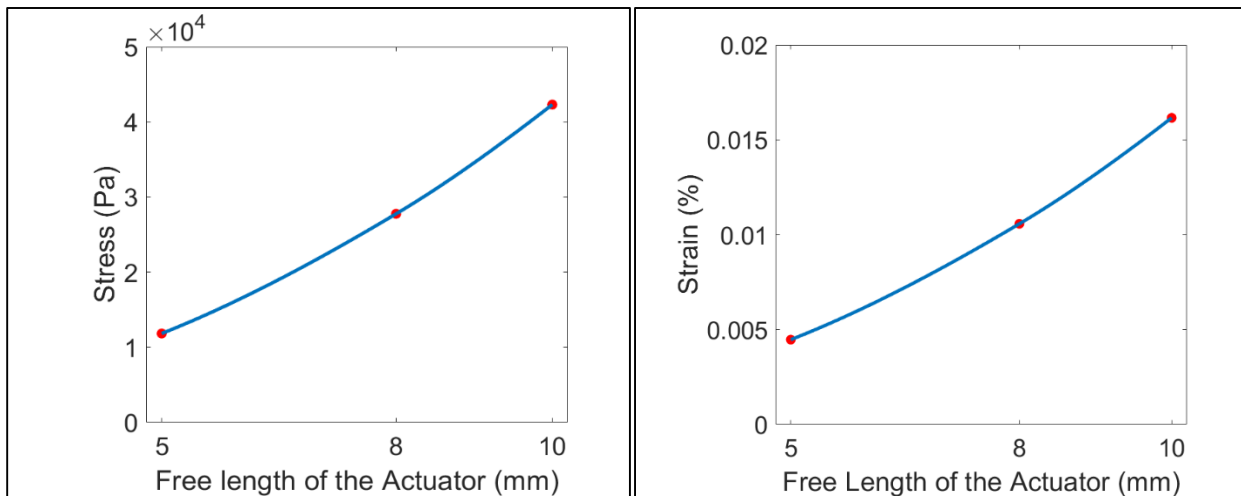
(b)

(c)

Figure 11: Mechanical response at different actuation length for the Nafion actuator: (a) Actuation length vs Displacement (b) Stress vs Actuation Length (c) Strain % vs Actuation Lengths

Chapter 5

Computational Result for TMD-Nafion Actuator

5.1 Introduction

In this Chapter, we study and present simulated results for a TMD-Nafion Actuator. The effect of incorporating TMDs in Nafion and how it improves the mechanical performance of the actuator have been studied. The geometry of the actuator is similar to the pure Nafion actuator shown in Chapter 4. However, the dimensions of the actuator are different and are presented in Table 3. These dimensions are taken from Loeian et al. [37] for the purpose of validating the simulated results with the experiments. To incorporate TMD in Nafion, we made some assumptions. It is shown in Loeian et al. [37] that the proton conductivity of the materials increases with increase in exfoliated TMDs in Nafion. So we increase the cation concentration of the Nafion model by the same ratio as proton conductivity to incorporate TMD. Also, the Young's Modulus is increased to 261.5 MPa as shown in Loeian et al. [37]. Now in order to get the desired displacement as close as possible to the experimental data from Loeian et al. [37], we adjust the diffusivity of the TMD-Nafion model. Initially, 2V square wave electric potential at 1Hz is applied to the actuator. All the other parameters shown in Table 4 are kept constant. Once we have the desired parameters for our model which produce the needed displacement. We simulate the results at different electric potential, frequencies and for various actuation lengths which are explained in detail in the following subsections of this chapter. The parameters that are used to define the TMD-Nafion actuator are shown in Table 4. In the case of an IPMC actuator, the displacement decreases with the increase in thickness and Young's modulus. But as seen in the results below, even with the

increase in thickness and Young's modulus, the TMD-Nafion actuator produces more displacement than the pure Nafion actuator. Also, it can be seen from the parameter that the diffusivity value for the TMD-Nafion actuator is more than the pure Nafion actuator. These shows that with the addition of the TMD there is an increase in the diffusivity which results in more bending and better actuation.

Free length of the actuator	10 mm
Length of the fixed part of the IPMC cantilever	3 mm
Thickness of the Actuator	0.093 mm
Thickness of the electrodes	0.0001 mm
Depth of the actuator (Width)	5 mm

Table 3: Geometric parameter of TMD-Nafion actuator.

Definition	Symbol (Used in Equations)	Symbol (As used in COMSOL)	Value	Units
Diffusivity or Diffusion constant	D	D_cat	1.7E-12	[m^2/s]
Charge Number	z	z_cat	1	
Gas constant	R	R	8.31	[J/(mol*K)]
Temperature	T	T	293	[K]
Cation concentration	C	conc_cat_conc	161	[mol/m^3]
Effective di-electric permittivity	ε	epsilon	2	[mF/m]

Density of the material	ρ_p	density_IPMC	2000	[kg/m^3]
Faraday constant	F	Faraday	96485.3415	[s*A/mol]
Young's Modulus	E	Young_IPMC	261.5	[Mpa]
Poisson's ratio	ν	Poission_IPMC	0.49	
Constant	α	Alpha	0.0001	[N/C]

Table 4: Parameters used in the modeling of the TMD-Nafion actuator

5.2 Simulation Results:

Figure 12 shows the graph of tip displacement of the actuator versus time. A 2V square signal at 1 Hz is applied to the actuator. The Length of the actuator was kept at 10mm. The high initial actuation is due to the electrochemical feedback which makes an initial fast electrically driven actuation followed by a slow actuation when the diffusive component of the chemical flux compensates for the effects of the electrical migrative component [58]. The displacement of the model is in good agreement with the experimental results. The model produces a displacement of ~ 0.151 mm at 2V for 10 mm actuation length in comparison to experimental displacement which is ~ 0.15 mm. Also, the displacement produced by TMD-Nafion (~ 0.151 mm at 2V 1 Hz Square wave) is more the pure Nafion actuator (~ 0.128 mm at 2V 1Hz square wave). Figure 13 shows the concentration of cation across the thickness of the actuator at 2V 1Hz square wave. As seen in Nafion actuator, there is a large increase in ion concentration in a small subsurface region (<1µm) which therefore causes swelling of the polymer near cathode and contraction near the anode. This, in turn, results in bending of the material towards the anode. The accumulation of ions at the surface of the composite causes the elongation of the surface and deformation of the actuator. We can also observe the increase in the cation concentration at the electrode-polymer interface for

TMD-Nafion actuator in comparison with the pure Nafion actuator. The bending in the actuator on the application of potential can be seen in figure 14. It also shows von Mises stress induced in the actuator due to the bending at 2V electric potential. The stress value here helps in analyzing the number of stress cycles the actuator can tolerate.

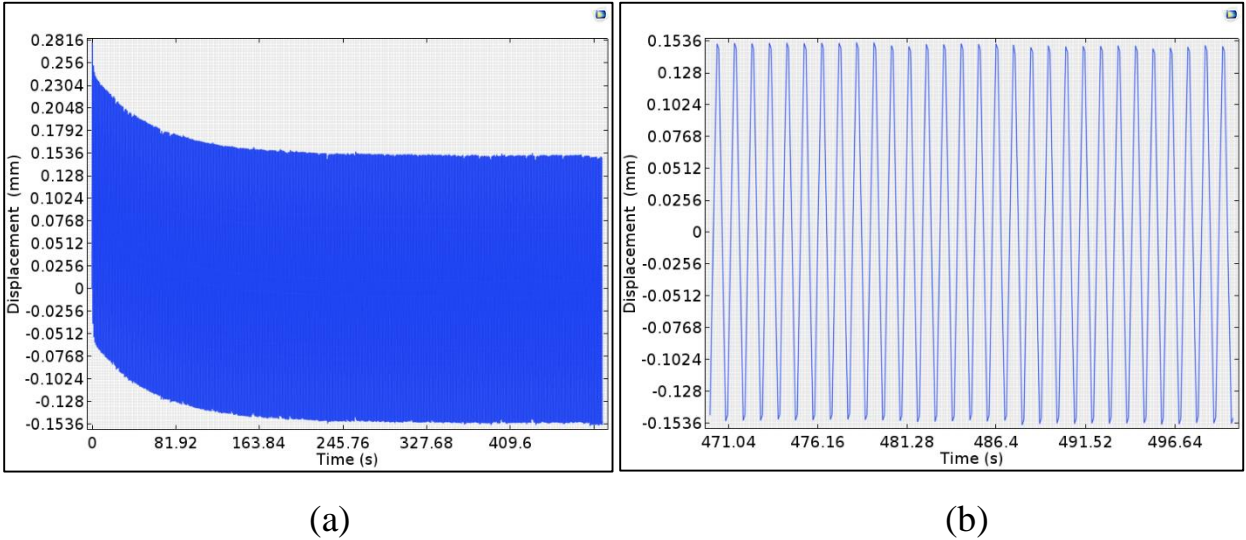(a)   (b)

Figure 12: Tip displacement of the TMD-Nafion actuator under applied potential.(a) Displacement vs Time under 2V 1Hz square signal (b) Zoomed image of the tip displacement
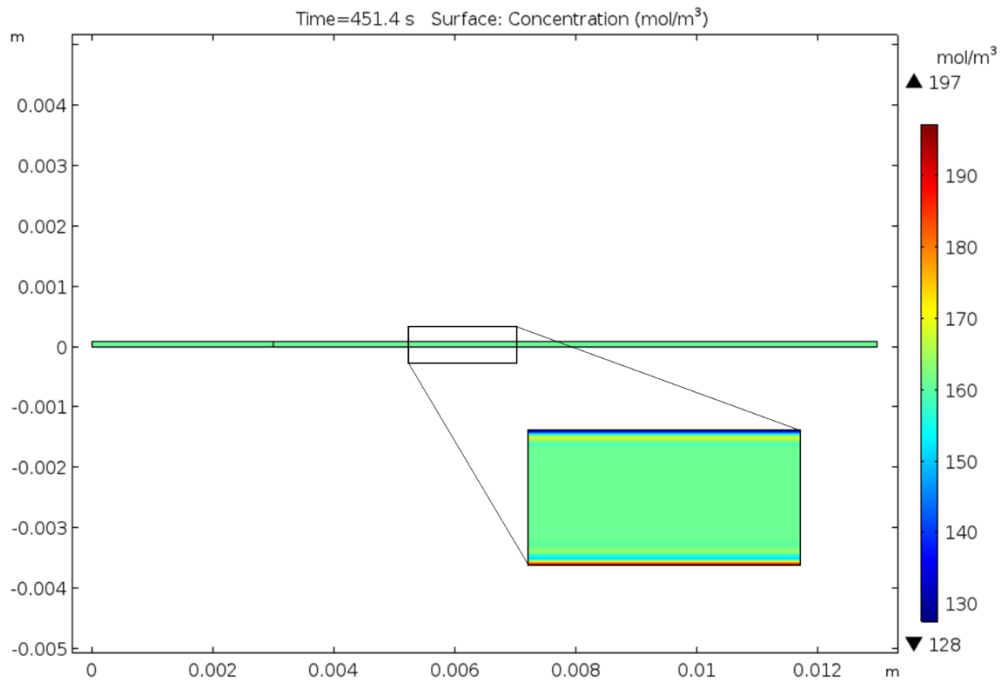
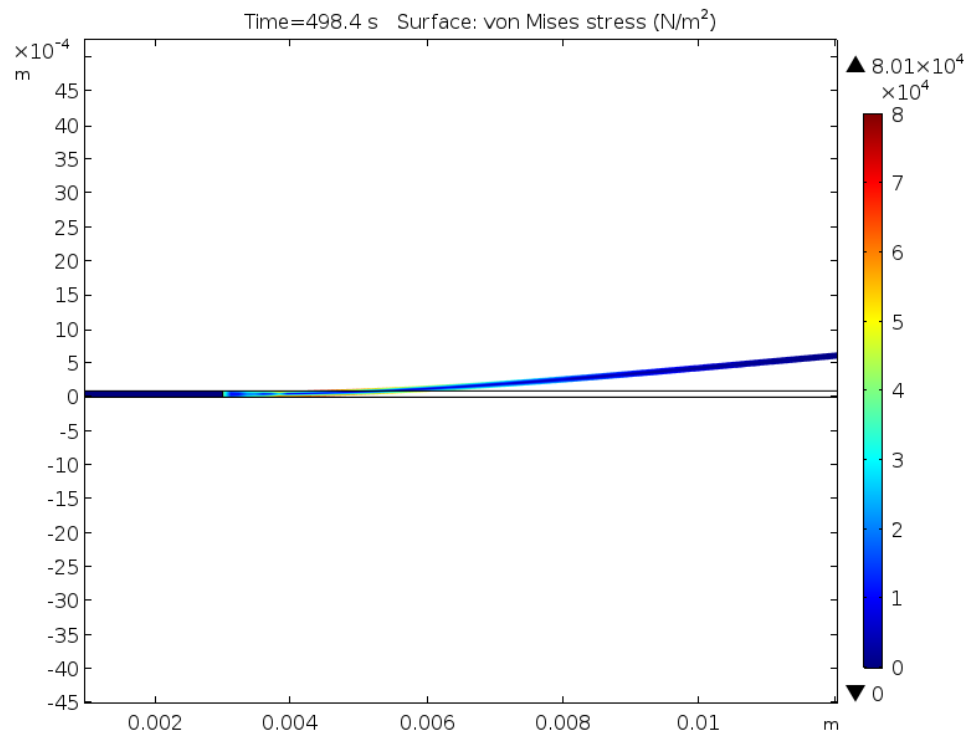*Figure 13: Cation concentration across the thickness of the TMD-Nafion actuator*

Figure 14: Von Mises Stress and bending of the TMD-Nafion actuator

5.3 Analyzing at Different Electric Potential

Here the actuator performance is analyzed at different electric potential as seen in Figure 15. The parameters of the actuator as shown in Table 4 is kept constant. The excitation frequency is kept at 1Hz, and the voltages are varied from 1V to 5V. The free length of the actuator was 10mm. Figure 15(a) shows displacement versus the electric potential for TMD-Nafion actuator. It can be seen that as the displacement increases with the increase in the electric potential. The stress and strain data with respect to the electric potential can be seen in Figure 15(b) and (c). As the potential increases, the stress as well as the strain increases. Table 5 shows the comparison between the experimental and simulated results for Nafion and TMD-Nafion actuator. We can see that there is an improvement in the displacement at all potential with the addition of TMDs. Also from Table 5, it can be seen that there is a slight deviation in the simulation results from the experiments. The difference can be due to the assumed values of cation concentration and diffusion constant. We had to assume these value since there was no data regarding it. So if we know the exact value of this parameter we can substitute them in the model and can get the required displacement.

(a)

<div align="center">(b)   (c)</div>
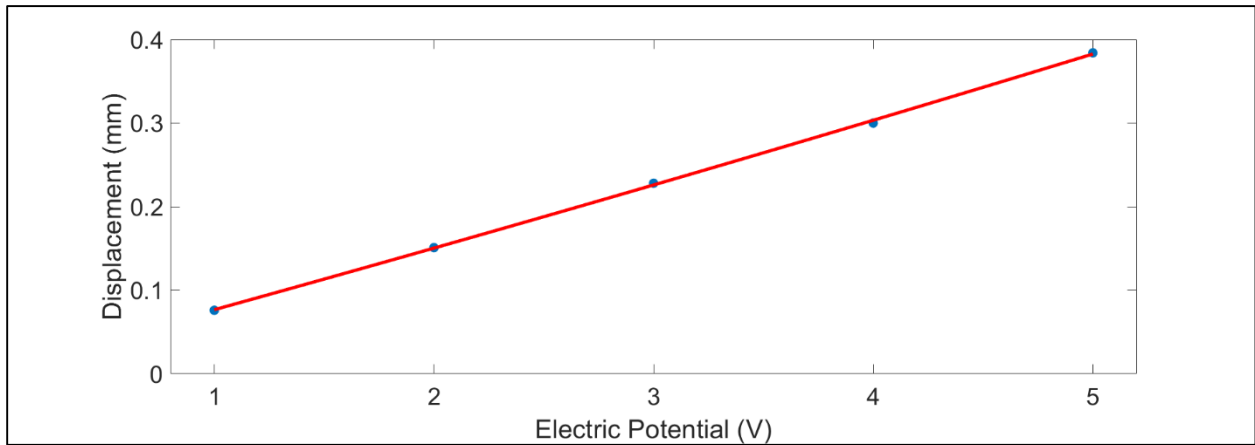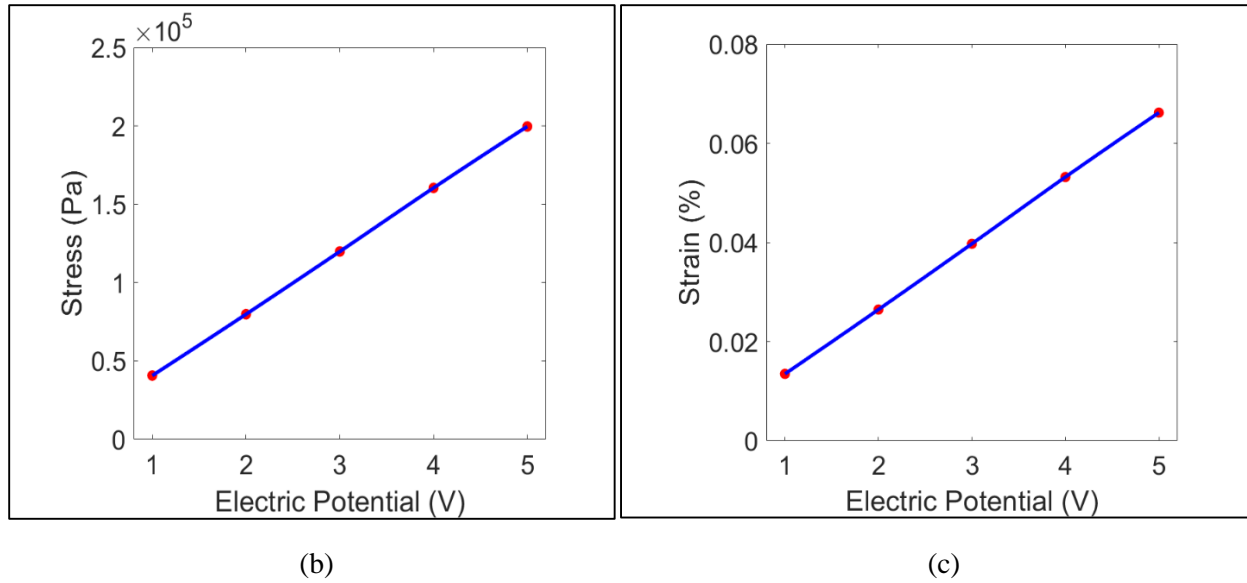
Figure 15: Mechanical response at different electric potential for TMD- Nafion actuator:(a)Displacement versus Electric potential (b) Stress versus Electric potential (c) Strain versus Electric Potential

Displacement (mm)			
Electric Potential (V)	Simulation Results (Nafion)	Simulation Results (TMD-Nafion)	Experimental Data(TMD-Nafion)
1	0.064	0.076	0.07
2	0.128	0.151	0.15
3	0.192	0.228	0.2
4	0.256	0.3	0.24
5	0.318	0.384	0.27

Table 5: Comparison of Experimental Data with the simulated data for Nafion and TMD-Nafion actuator for displacement at different electric potentials

5.4 Analyzing at Different Excitation Frequencies

Here we analyze the actuator at various excitation frequencies as seen in figure 16. The applied electric potential amplitude was kept at 2V for all frequencies. The actuation length is kept at 10 mm. Performance is studied at 0.1 Hz,1Hz, and 5Hz. Figure 16(a) shows how the displacement varies with the excitation frequencies. It is seen that as the excitation frequency increases the

<div align="center">32</div>

displacement of the actuator decreases. The stress and strain relationships with the excitation frequency can be seen in Figure 16(b) and (c) respectively. The improvement in the actuation can be seen when compared with the results for the pure Nafion actuator.
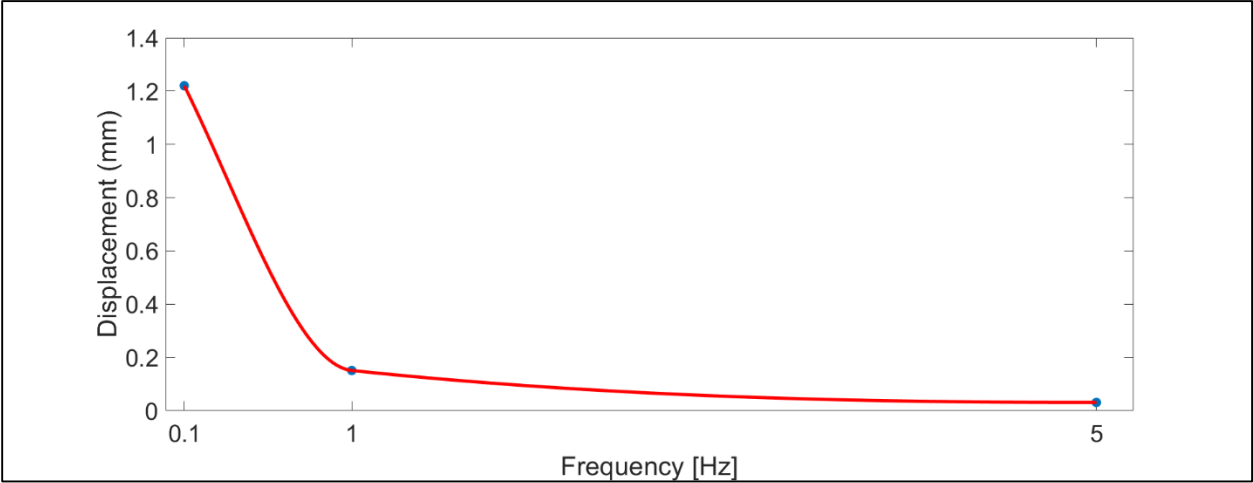
(a)
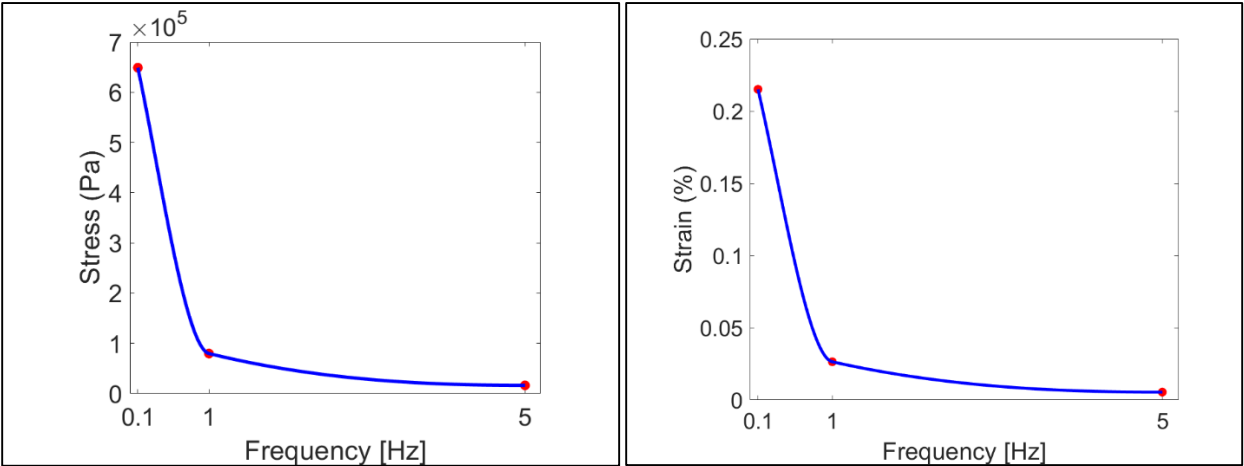
(b)

(c)

Figure 16: Mechanical response at different excitation frequencies for TMD-Nafion actuator:(a)Displacement versus frequency(b) Stress versus frequency (c) Strain % versus frequency

5.5 Effect of Varying Actuation Lengths

Here we analyze the actuator at different actuation lengths. The electric potential amplitude was kept at 2V 1 Hz for all actuators. Actuation length of 5mm, 8mm, and 10mm were used to study the performance. Figure 17(a) shows the displacement versus actuation length plot. The displacement decreases with the decrease in the actuation length. When compared with the results of pure Nafion actuator model you can observe the increase in the displacement of the actuator for the same lengths. The parameters were kept constant for all the samples. The stress and strain relation for various length of the actuator can be seen in Figure 17(b) and (c) respectively. Also, as the actuation length increases the stress and strain increases. The stress and strain values obtained were also higher for TMD-Nafion actuator as compared to Nafion.

(a)
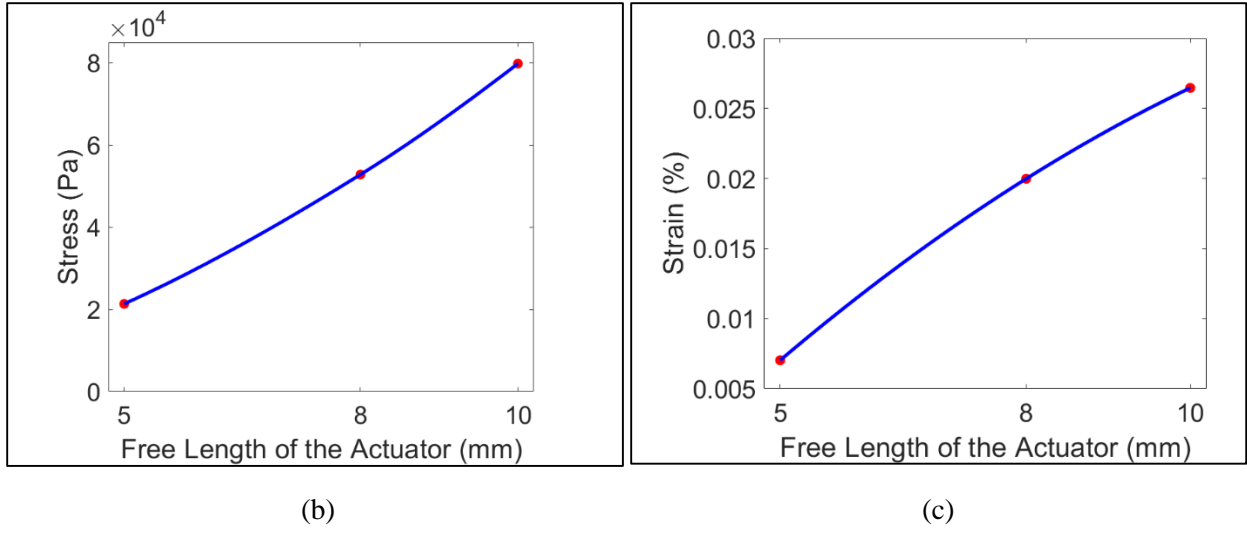
(b)   (c)
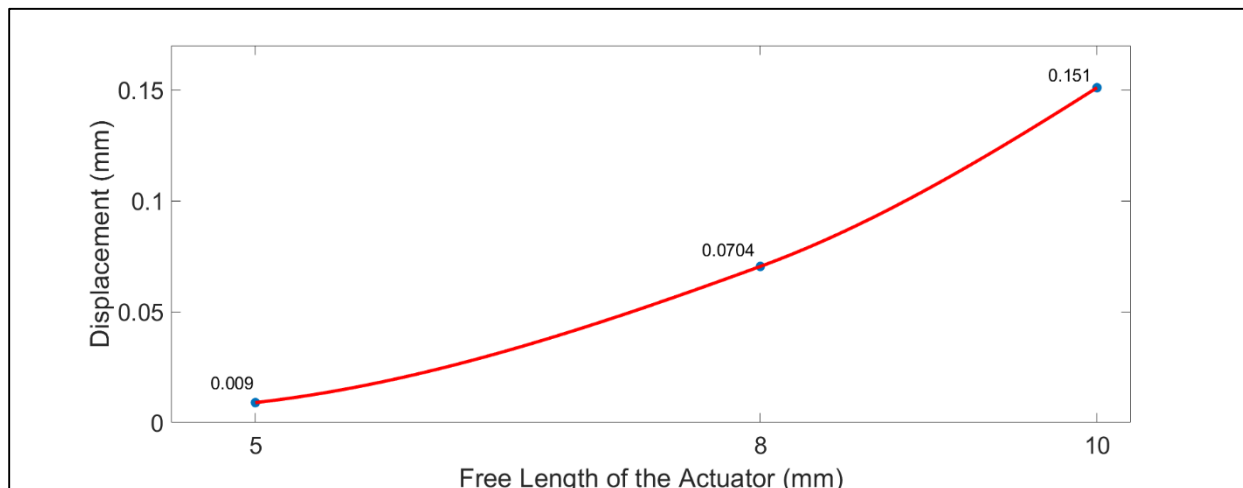
Figure 17: Mechanical response at different actuation length for the TMD-Nafion actuator: (a) Actuation length vs Displacement (b) Stress vs Actuation Length (c) Strain % vs Actuation Lengths.

Chapter 6

Conclusion and Future Directions

The ability to convert electrical energy into mechanical motion is one of the fundamental building blocks for modern day actuators. The efforts in recent years have been towards understanding various nanomaterials such as carbon nanotubes and graphene in polymers. For the first time, we show interesting effects of incorporating TMDs such as WS2 in Nafion and demonstrate the improvement in the electromechanical actuation performance. The most common TMD namely MoS2 share similar structure as WS2 and are hydrophilic. This opens a broader field of applications of different types of TMDs (MoS2, WS2, MoTe2, etc.) for electrochemical or electromechanical actuation.

In this study, we first developed the model for TMD-Nafion based electromechanical actuator in COMSOL Multi-Physics software. The experimental results were validated with the simulation and showed good agreement. It was seen that the addition of TMDs in Nafion improved the actuation performance of the actuator. We were able to obtain more displacement of the actuator for the same actuation length. Also, the stress and the strain values are higher than the pure Nafion based actuator. It was also seen that even with the increase in the thickness and Young's modulus of the actuator due to which the displacement of the actuator decreases we were able to obtain more displacement. This shows how the addition of TMDs improves the actuation performance of the actuator. In the future, if the exact value of the diffusivity and cation concentration are obtained we can get the accurate displacement for the actuator from the model. The effect of meshing can

be analyzed so as how the meshing techniques affects the results of the actuator model. Also, in order to have more insights on the underlying mechanism of the actuator the model can be solved using numerical methods which would help in understanding how the equations work for solving the model.

References

1. Petersen, A. Piezoelectric Actuators. F M-Feinwerktech Mes 86, 304–308 (1978).
2. Park, S. E. & Shrout, T. R. Ultrahigh strain and piezoelectric behavior in relaxor based ferroelectric single crystals. Journal of Applied Physics 82, 1804–1811, https://doi.org/10.1063/1.365983 (1997).
3. Hashimoto, M., Takeda, M., Sagawa, H., Chiba, I. & Sato, K. Application of Shape Memory Alloy to Robotic Actuators. J Robotic Syst2, 3–25 (1985).
4. Hirai, M. et al. Electrically-Induced Reversible Structural-Change of a Highly Swollen Polymer Gel Network. J Chem Soc Faraday T 91, 473–477, https://doi.org/10.1039/ft9959100473 (1995).
5. Bar-Cohen, Y., Xue, T., Shahinpoor, M., Simpson, J. O. & Smith, J. Low-mass muscle actuators using electroactive polymers (EAP). Smart Structures and Materials 1998: SmartMaterials Technologies 3324, 218–223, https://doi.org/10.1117/12.316866 (1998).
6. Shahinpoor, M., Bar-Cohen, Y., Xue, T., Simpson, J. O. & Smith, J. Some experimental results on ionic polymer-metal composites(IPMC) as biomimetic sensors and actuators. Smart Structures and Materials 1998: SmartMaterials Technologies 3324, 251–267, https://doi.org/10.1117/12.316870 (1998).
7. Pelrine, R., Kornbluh, R., Pei, Q. B. & Joseph, J. High-speed electrically actuated elastomers with strain greater than 100%. Science 287, 836–839, https://doi.org/10.1126/science.287.5454.836 (2000).
8. K. Oguro, Y. Kawami, and H. Takenaka, "Bending of an ion-conducting polymer film-electrode composite by an electric stimulus at low voltage," Journal of Micromachine Society, vol. 5, no. 1, pp. 27–30, 1992.
9. Shahinpoor, M., & Kim, K. J. (2001). Ionic polymer-metal composites: I. Fundamentals. Smart materials and structures, 10(4), 819.
10. Nemat-Nasser, S., & Wu, Y. (2003). Comparative experimental study of ionic polymer–metal composites with different backbone ionomers and in various cation forms. Journal of Applied Physics, 93(9), 5255-5267.
11. Pugal, D., Kim, K. J., Punning, A., Kasemägi, H., Kruusmaa, M., & Aabloo, A. (2008). A self-oscillating ionic polymer-metal composite bending actuator. Journal of Applied Physics, 103(8), 084908.
12. Nemat-Nasser, S., & Li, J. Y. (2000). Electromechanical response of ionic polymer-metal composites. Journal of Applied Physics, 87(7), 3321-3331.
13. Kim, G., Kim, H., Kim, I. J., Kim, J. R., Lee, J. I., & Ree, M. (2009). Bacterial adhesion, cell adhesion and biocompatibility of Nafion films. *Journal of Biomaterials Science, Polymer Edition*, *20*(12), 1687-1707.
14. Gerritsen, M., Kros, A., Sprakel, V., Lutterman, J. A., Nolte, R. J. M., & Jansen, J. A. (2000). Biocompatibility evaluation of sol–gel coatings for subcutaneously implantable glucose sensors. *Biomaterials*, *21*(1), 71-78.
15. Iijima, S. & Ichihashi, T. Single-Shell Carbon Nanotubes of 1-Nm Diameter (Vol 363, Pg 603, 1993). *Nature* **364**, 737–737 (1993).

16. Novoselov, K. S., Geim, A. K., Morozov, S. V., Jiang, D. A., Zhang, Y., Dubonos, S. V., ... & Firsov, A. A. (2004). Electric field effect in atomically thin carbon films. *science*, *306*(5696), 666-669.

17. Baughman, R. H., Cui, C., Zakhidov, A. A., Iqbal, Z., Barisci, J. N., Spinks, G. M., ... & Jaschinski, O. (1999). Carbon nanotube actuators. *Science*, *284*(5418), 1340-1344.

18. Chen, L., Liu, C., Liu, K., Meng, C., Hu, C., Wang, J., & Fan, S. (2011). High-performance, low-voltage, and easy-operable bending actuator based on aligned carbon nanotube/polymer composites. *ACS nano*, *5*(3), 1588-1593.

19. Landi, B. J., Raffaelle, R. P., Heben, M. J., Alleman, J. L., VanDerveer, W., & Gennett, T. (2002). Single wall carbon nanotube− nafion composite actuators. *Nano Letters*, *2*(11), 1329-1332.

20. Jung, J. H., Jeon, J. H., Sridhar, V., & Oh, I. K. (2011). Electro-active graphene–Nafion actuators. *Carbon*, *49*(4), 1279-1289.

21. Bian, K., Liu, H., Tai, G., Zhu, K., & Xiong, K. (2016). Enhanced actuation response of nafion-based ionic polymer metal composites by doping BaTiO3 nanoparticles. *The Journal of Physical Chemistry C*, *120*(23), 12377-12384.

22. Grot, W. G. F., Mehra, V., Munn, G. E. & Solenberger, J. C. Nafion Electrolytic Separators. *J Electrochem Soc* **122**, C104–C104 (1975).

23. Hora, C. J. & Maloney, D. E. Chemically Modified Nafion Perfluorosulfonic Acid Membranes as Separators in Chlor-Alkali Cells. J Electrochem Soc 124, C319–C319 (1977).

24. Pu, C., Huang, W., Ley, K. L., & Smotkin, E. S. (1995). A methanol impermeable proton conducting composite electrolyte system. *Journal of the Electrochemical Society*, *142*(7), L119-L120.

25. Bath, B. D., Lee, R. D., White, H. S., & Scott, E. R. (1998). Imaging molecular transport in porous membranes. Observation and analysis of electroosmotic flow in individual pores using the scanning electrochemical microscope. *Analytical chemistry*, *70*(6), 1047-1058.

26. Honda, K., & Hayashi, H. (1987). Prussian Blue containing nafion composite film as rechargeable battery. *Journal of The Electrochemical Society*, *134*(6), 1330-1334.

27. Schmidt-Rohr, K. & Chen, Q. Parallel cylindrical water nanochannels in Nafion fuel-cell membranes. *Nat Mater* **7**, 75–83, (2008).

28. Radisavljevic, B., Radenovic, A., Brivio, J., Giacometti, I. V., & Kis, A. (2011). Single-layer MoS 2 transistors. *Nature nanotechnology*, *6*(3), 147.

29. Lopez-Sanchez, O., Lembke, D., Kayci, M., Radenovic, A., & Kis, A. (2013). Ultrasensitive photodetectors based on monolayer MoS 2. *Nature nanotechnology*, *8*(7), 497.

30. Rahneshin, V., Khosravi, F., Ziolkowska, D. A., Jasinski, J. B., & Panchapakesan, B. (2016). Chromatic mechanical response in 2-D layered transition metal dichalcogenide (TMDs) based nanocomposites. *Scientific reports*, *6*, 34831.

31. Tsai, M. L., Su, S. H., Chang, J. K., Tsai, D. S., Chen, C. H., Wu, C. I., ... & He, J. H. (2014). Monolayer MoS2 heterojunction solar cells. *ACS nano*, *8*(8), 8317-8322.

32. Mak, K. F., Lee, C., Hone, J., Shan, J., & Heinz, T. F. (2010). Atomically thin MoS 2: a new direct-gap semiconductor. *Physical review letters*, *105*(13), 136805.

33. Li, H., Yin, Z., He, Q., Li, H., Huang, X., Lu, G., ... & Zhang, H. (2012). Fabrication of single- and multilayer MoS2 film-based field-effect transistors for sensing NO at room temperature. *small*, *8*(1), 63-67.

34. Lukowski, M. A., Daniel, A. S., Meng, F., Forticaux, A., Li, L., & Jin, S. (2013). Enhanced hydrogen evolution catalysis from chemically exfoliated metallic MoS2 nanosheets. *Journal of the American Chemical Society*, *135*(28), 10274-10277.

35. Wang, T., Chen, S., Pang, H., Xue, H., & Yu, Y. (2017). MoS2-Based Nanocomposites for Electrochemical Energy Storage. *Advanced Science*, *4*(2), 1600289.

36. Fan, X., Khosravi, F., Rahneshin, V., Shanmugam, M., Loeian, M., Jasinski, J., ... & Panchapakesan, B. (2015). MoS2 actuators: reversible mechanical responses of MoS2-polymer nanocomposites to photons. *Nanotechnology*, *26*(26), 261001.

37. Loeian, M. S., Ziolkowska, D. A., Khosravi, F., Jasinski, J. B., & Panchapakesan, B. (2017). Exfoliated WS 2-Nafion Composite based Electromechanical Actuators. *Scientific reports*, *7*(1), 14599.

38. Segalman, D. J., Witkowski, W. R., Adolf, D. B., & Shahinpoor, M. (1992). Theory and application of electrically controlled polymeric gels. *Smart Materials and Structures*, *1*(1), 95.

39. Shahinpoor, M. (1992). Conceptual design, kinematics and dynamics of swimming robotic structures using ionic polymeric gel muscles. *Smart Materials and Structures*, *1*(1), 91.

40. Segalman, D., Witkowski, W., Adolf, D., & Shahinpoor, M. (1991, November). ELECTBICALLY CONTROLLED POLYMERIC MUSCLES AS ACTIVE MATERIALS USED IN ADAPTIVE STRUCTURES. In *An International Symposium & Exhibition on Active Materials & Adaptive Structures* (p. 162).

41. Segalman, D. J., Witkowski, W. R., Rao, R. R., Adolf, D. B., & Shahinpoor, M. (1993, July). Finite element simulation of the 2D collapse of a polyelectrolyte gel disk. In *Smart Structures and Materials 1993: Smart Materials* (Vol. 1916, pp. 14-22). International Society for Optics and Photonics.

42. Segalman, D. J., & Witkowski, W. R. (1995). Two-dimensional finite element analysis of a polymer gel drug delivery system. *Materials Science and Engineering: C*, *2*(4), 243-249.

43. Shahinpoor, M. (1993). Electro-mechanics of bending of ionic polymeric gels as synthetic muscles for adaptive structures. *ASME-PUBLICATIONS-AD*, *35*, 11-11.

44. Shahinpoor, M. (1994). Continuum electromechanics of ionic polymeric gels as artificial muscles for robotic applications. *Smart Materials and Structures*, *3*(3), 367.

45. Shahinpoor, M. (1995). Micro-electro-mechanics of ionic polymeric gels as electrically controllable artificial muscles. *Journal of Intelligent Material Systems and Structures*, *6*(3), 307-314.

46. De Gennes, P. G., Okumura, K., Shahinpoor, M., & Kim, K. J. (2000). Mechanoelectric effects in ionic gels. *EPL (Europhysics Letters)*, *50*(4), 513.

47. Li, J. Y., & Nemat-Nasser, S. (2000). Micromechanical analysis of ionic clustering in Nafion perfluorinated membrane. *Mechanics of materials*, *32*(5), 303-314.

48. Akle, B. J., Leo, D. J., Hickner, M. A., & McGrath, J. E. (2005). Correlation of capacitance and actuation in ionomeric polymer transducers. *Journal of Materials Science*, *40*(14), 3715-3724.

49. Toi, Y., & Kang, S. S. (2005). Finite element analysis of two-dimensional electrochemical–mechanical response of ionic conducting polymer–metal composite beams. *Computers & structures*, *83*(31-32), 2573-2583.

50. Wallmersperger, T., Akle, B. J., Leo, D. J., & Kröplin, B. (2008). Electrochemical response in ionic polymer transducers: An experimental and theoretical study. *Composites Science and Technology*, *68*(5), 1173-1180.

51. Akle, B. J., Habchi, W., Wallmersperger, T., Akle, E. J., & Leo, D. J. (2011). High surface area electrodes in ionic polymer transducers: numerical and experimental investigations of the electro-chemical behavior. *Journal of Applied Physics*, *109*(7), 074509.

52. Pugal, D., Kim, K. J., & Aabloo, A. (2011). An explicit physics-based model of ionic polymer-metal composite actuators. *Journal of Applied Physics*, *110*(8), 084904.

53. Martinez, M., & Lumia, R. (2013). Distributed force simulation for arbitrarily shaped IPMC actuators. *Smart Materials and Structures*, *22*(7), 075024.

54. Vokoun, D., He, Q., Heller, L., Yu, M., & Dai, Z. (2015). Modeling of IPMC cantilever's displacements and blocking forces. *Journal of Bionic Engineering*, *12*(1), 142-151.

55. Nam, D. N. C., & Ahn, K. K. (2014). Analysis and experiment on a self-sensing ionic polymer–metal composite actuator. *Smart Materials and Structures*, *23*(7), 074007.

56. Pugal, D. (2012). *Physics based model of ionic polymer-metal composite electromechanical and mechanoelectrical transduction*. University of Nevada, Reno.

57. Grimshaw, P. E., Nussbaum, J. H., Grodzinsky, A. J., & Yarmush, M. L. (1990). Kinetics of electrically and chemically induced swelling in polyelectrolyte gels. *The Journal of Chemical Physics*, *93*(6), 4462-4472.

58. Ranjbarzadeh, S. (2017). *MODELING, SIMULATION AND APPLICATIONS OF IONIC POLYMER METAL COMPOSITES*(Doctoral dissertation, Universidade Federal do Rio de Janeiro).